Master of Science Thesis

Complementary analysis of breast cancer using MRI and breast tomosynthesis

Daniel Förnvik

Supervisors: Anders Tingberg, Associate Professor,
Mark Ruschin, PhD

The work has been performed at the
Department of Radiation Physics
Malmö University Hospital

Medical Radiation Physics
Clinical Sciences, Lund
Lund University, 2008

Abstract

The purpose of this work is to explore and quantify physical metrics of breast tumors in both magnetic resonance imaging (MRI) and breast tomosynthesis (BT) images, and relate these metrics to pathophysiological and histopathological findings.

An analysis of breast specimens containing tumors will be employed to determine BT metrics of interest. These metrics will then be applied to patient images to test whether they are suitable in predicting malignancy or not. Clinical images of 10 patients who have undergone both MRI and BT examinations have been obtained and studied in this project.

The tumors seen in the tomosynthesis slices were characterized by objective measures such as *degree of spiculation*, *irregularity* and *size*. These measures were compared to contrast uptake curves created from the respective tumors in the MR images.

Two different MRI methods (*wash-in/wash-out* and *persistent curve type percentage*) were established and compared. Both methods have a sensitivity of 100% but the specificity is higher for the *persistent curve type percentage* method. With regards to the BT metrics, the parameters *irregularity* and *ellipticity* both had a significant difference between malignant and benign cases. No relationship was observed in the inter-metric analysis of the BT and MRI metrics, however, not enough data was available to draw any conclusions.

The results indicate that the BT parameters *irregularity* and *ellipticity* may be useful for differentiation between malignant and benign tumors.

Contents

1 Introduction

Breast cancer is the most common form of female cancer in Sweden, with around 7000 women diagnosed annually. It is also the second most common cause of death amongst women aged 45-74 after death from cardiovascular diseases. Each year around 1600 deaths are caused by malignant breast tumors [1].

The introduction of mammography screening of the female population has reduced the mortality associated with breast cancer [2-3]. Conventional mammography is a two-dimensional (2D) X-ray imaging technique. More recently, a novel form of digital mammography has been introduced, referred to as breast tomosynthesis (BT) [4]. BT differs from conventional 2D mammography in that it is a tomographic technique and provides information about the breast in three dimensions. Consequently, it reduces the problem of superimposed anatomical structures by allowing retrospective reconstruction of an arbitrary number of tomographic slices. In addition, approximately the same absorbed dose is used for a BT examination as for a conventional mammography examination, although the optimal dose level is still under investigation [5]. The evaluation of BT as a future breast screening modality is currently a pioneering field of research.

Another modality that has gained acceptance in research as a complementary investigation tool to the standard 2D X-ray mammography, is dynamic contrast-enhanced breast magnetic resonance imaging (DCE-MRI) [6-8]. In addition to morphological information, DCE-MRI is based on the presence of neovascularization, which can be used to distinguish between malignant and benign tumors. Adding breast MRI to mammography provides a superior sensitivity compared to mammography alone, with or without breast ultrasound [9]. However, the specificity is still rather low, resulting in a higher rate of investigation of false-positive findings. This leads to decreased patient throughput and increased costs of imaging. The cost, time aspects and specificity limit the use of MRI in the diagnosis of breast disease. Hence, it is too complicated to implement in a population based screening, but can be used for screening of high risk groups [10].

The purpose of this work is to explore and quantify physical metrics of breast tumors in both MRI and BT images, and relate these metrics to pathophysiological and histopathological findings. An analysis of breast specimens will be employed to determine BT metrics of interest. The specimen images contain clearer tumor characteristics and less noise as they have been obtained with higher tube loading than the patient images. These metrics will then be applied to patient images to test whether they are suitable in predicting malignancy or not.

The patient group has undergone both DCE-MRI, BT and pathological anatomical diagnosis (PAD). The tumors seen in the tomosynthesis slices will be characterized by objective measures such as degree of spiculation, irregularity and size, and these measures will be compared to contrast uptake metrics created from the respective tumors in the MR images.

2 Theory

2.1 Breast Tomosynthesis

The introduction of large flat-panel detectors with high detective quantum efficiency and rapid read-out together with more powerful computers and reconstruction software in the last decade has made the development of BT possible [11]. With this technique, the 3D breast volume is obtained through a mathematical reconstruction of the multiple projection images, acquired over an angular range of typically ±12-25°, to slices parallel to the detector plane (Figure 1). Typically, this is done employing a filtered backprojection algorithm [12] and a BT image set is shown in Figure 2.

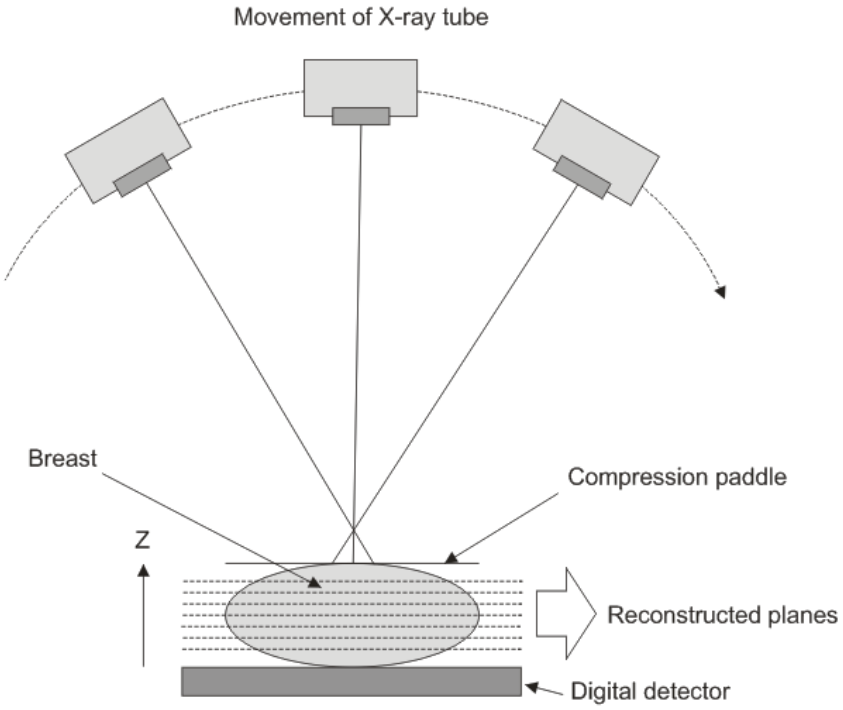

Figure 1: Schematic illustration of breast tomosynthesis. Multiple projections are acquired during the X-ray tube movement. Only three projections are shown for simplicity.

The high spatial resolution of mammograms in two dimensions is almost completely retained for the BT system (70 μm for mammograms [13] and 85 μm for BT [4]). However, for the BT system there is also a third dimension after reconstruction with a typical slice thickness of 1 mm. Since the angular range and number of projections are limited, the frequency component in the z-dimension will be undersampled leading to artifacts in the reconstructed images [14]. Nevertheless, previous studies have indicated that tumor visibility is higher in BT images than in digital mammographic X-ray imaging, due to the reduction of anatomical noise [15-16].

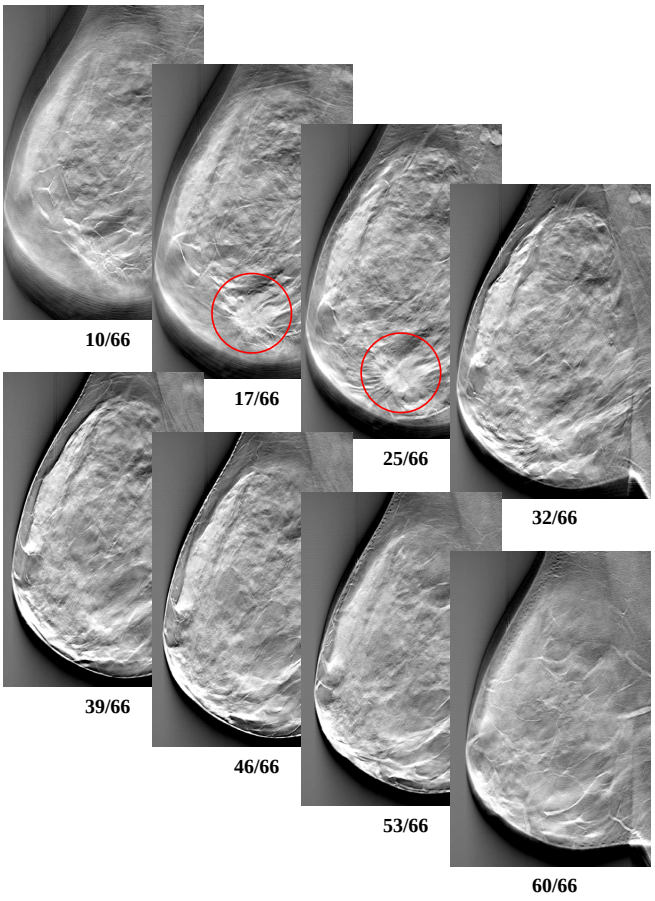

Figure 2: Example of a BT image set. 8 of 66 slices that build up the 3D volume are shown. Note the large tumor in the lower region of the breast that is clearly visible in slice 17 and 25. Each slice is roughly 1 mm thick.

Another advantage with BT is that the examination can be performed relatively fast with the whole series of projections being acquired in seconds.

2.2 Radiographic manifestations and histological grading of breast cancer

The radiographic findings in breast cancer are related to the local manifestations of neoplastic cell proliferation. Like other types of cancer, breast cancer is a heterogeneous disease and the appearance can differ in many ways. The radiographic findings can be categorized into two large groups, masses and microcalcifications. The main focus in this study is on masses.

Several histologic classifications of breast cancer types exist [17], but for the purpose of this study the basic classification in Table 1 was used.

Table 1: Histologic classification of breast carcinoma for the purpose of this study.

Invasive carcinoma
Ductal
Lobular
Tubular
Others
Noninvasive carcinoma
DCIS
LCIS

DCIS: ductal carcinoma in situ, *LCIS*: lobular carcinoma in situ

The majority of breast cancers arise in the cells lining the ductal system of the breast and are called ductal carcinomas. Cancers confined to the ducts themselves are called in situ carcinomas. Once the tumor has extended beyond the duct lumen, the term invasive carcinoma is applied. Invasive ductal carcinomas correspond to approximately 70% of all breast cancers. About 10% is comprised of invasive lobular carcinoma, 1-5% invasive tubular carcinoma and others account for about 5-10% [17-18].

The term "ductal" refers to cancers that originate from ductal epithelium as opposed to "lobular" carcinoma, which were thought to develop in the lobules. However, nowadays both types of cancer are believed to originate in the terminal lobular-ductal unit of the breast gland. The difference between the types now refers to the growth pattern, ductal carcinomas grow in columns without the formation of organoid structures such as tubular or papillary structures while lobular carcinomas often grow in single rows diffusely infiltrating the normal breast structures [17].

Examples of mass lesions seen with BT are shown in Figure 3.

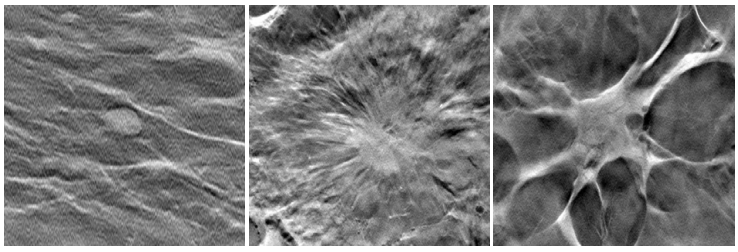

Figure 3: Example of mass lesions seen with BT. From left to right: circumscribed benign mass found to be a hamartoma; indistinct, spiculated malignant mass found to be invasive lobular carcinoma; spiculated malignant mass found to be invasive ductal carcinoma.

The grade, or state of aggressiveness, of any cancer is an important piece of information needed by physicians who treat cancer. For example the TNM staging system is widely used for all types of cancer, but more specific histological grading systems such as that described by Elston *et al.*, often referred to as the Nottingham grading system [19], are especially used

for breast cancer. These tumor grading systems combine nuclear variation, tubule formation and mitotic rate. The morphological findings are assessed with either cytology or histology.

The Nottingham grading system is shown in Figure 4. Each element is given a score of 1 to 3 and the score of all three components are added together to give the histological grade. The lowest possible score (1+1+1=3) is given to well differentiated tumors that all form tubules and have a low mitotic rate. The highest possible score is 9 (3+3+3=9). Dalton *et al.* [20] constructed survival curves for the Nottingham scores grouped according to the level at which pathologists tend to agree in assessing grade, and showed that the probability of patient survival is lowest for the high grade and highest for the low grade cancer types.

The Nottingham histological grading system can be combined with size and axillary status into a prognostic index. Tumor size is therefore an important parameter to examine.

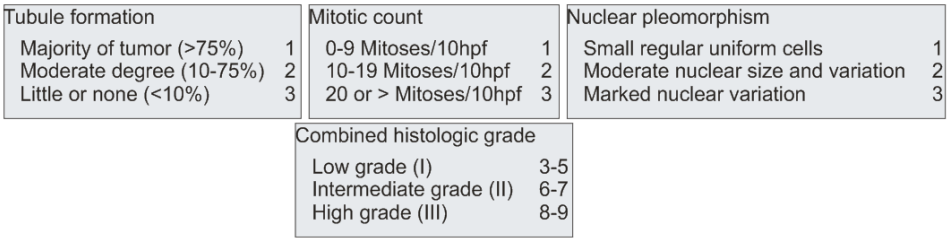

Figure 4: The Nottingham grading system. (hpf stands for high power field, the area visible under the maximum magnification power of the objective being used)

2.2.1 Feature extraction

Radiographically, mass lesions can be classified by various characteristics including degree of spiculation, margin of the mass, shape, homogeneity and density. These characteristics are used by radiologists to distinguish between malignant and benign masses. In this work, focus will be put on tumor margin and shape and a schematic illustration is shown in Figure 5.

The most common type of breast cancer is the spiculated lesion, accounting for about 60% of all breast cancers detected [21]. Seven percent of the malignant lesions are well-defined (circumscribed) densities. This means that well-defined masses can still be malignant, although most well-defined masses are benign.

Spiculation corresponds to the outward growth of a malignancy combined with a reactive fibrosis, resulting from a thickening of the fibrous structures around the tumor. The more irregular the margin of a mass is, the more suspicious it is for malignancy. The same is true for masses which are more lobulated [22]. In the preoperative treatment planning, accurate determination of the size of a breast tumor is important, in particular with the increased use of breast-saving surgery [23]. In this respect, there could be widespread discrepancies between lesion size evaluated on imaging modalities and sizes recorded in clinical examinations and by pathologists. Differences in size have been noted between various diagnostic modalities [24]. Comparing BT and MR in this respect would be an interesting future project.

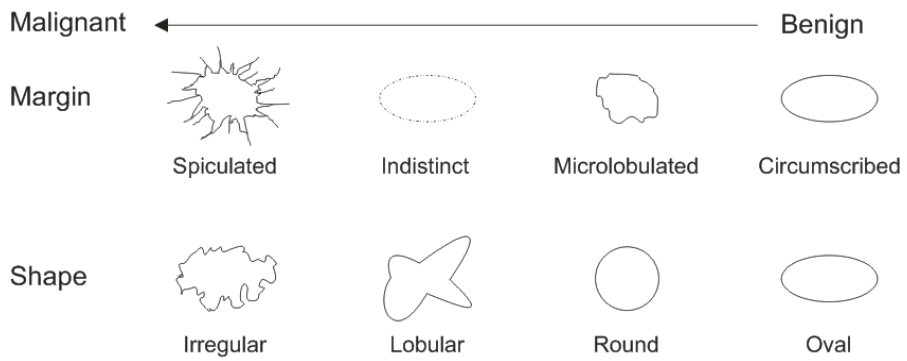

Figure 5: Schematic illustration of morphological features exhibited by mass lesions on mammograms [18].

The parameters evaluated for BT will be irregularity, ellipticity and degree of spiculation. Irregularity and ellipticity relate to the shape and degree of spiculation relates to the margin of the lesion. A schematic illustration of geometric features related to lesion shape is shown in Figure 6. How the geometric features are retrieved is described in 3.1.

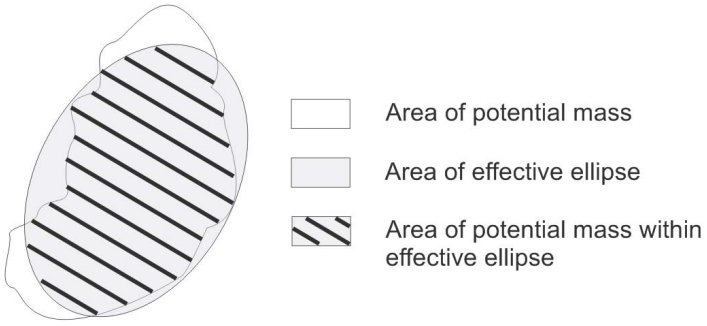

Figure 6: Geometric features related to lesion shape include irregularity and ellipticity. The area of potential mass and the area of effective ellipse are equal [18].

Irregularity is defined and calculated according to Equation 1.

$$Irregularity = 1 - \frac{perimeter\ of\ effective\ ellipse}{perimeter\ of\ potential\ mass} \tag{1}$$

Ellipticity is defined and calculated according to Equation 2.

$$Ellipticity = \frac{area\ of\ potential\ mass\ within\ effective\ ellipse}{area\ of\ potential\ mass} \tag{2}$$

In order to extract margin information from a mass lesion, the image of the mass lesion has to undergo a blurring (smoothing) process. The blurred mass lesion image is obtained by morphological filtering using sequences of dilation and erosion [25]. The basic effect of

the dilation operator on a binary image is to gradually enlarge the boundaries of regions of foreground pixels. Thus areas of foreground pixels grow in size while holes within those regions become smaller. This can be expressed as Equation 3.

$$A \oplus B = \{x|(\widehat{B})_x \cap A \neq \emptyset\} \tag{3}$$

The dilation of A and B expands A with B.

In a similar fashion the basic effect of the erosion operator on a binary image is instead to erode away the boundaries of regions of foreground pixels. Thus areas of foreground pixels shrink in size, and holes within those areas become larger. This can be expressed as Equation 4.

$$A \ominus B = \{x|(\widehat{B})_x \subseteq A\} \tag{4}$$

The erosion of A and B erodes A with B.

The areas of the original lesion and the blurred lesion are determined in terms of number of pixels. The difference between the areas of the two lesions is calculated and normalized to the original lesion. The area is expected to be less for the smooth lesion than the original lesion since the blurring of the original lesion results in a reduction of any spiculations in the margin. A large difference in the areas between the original lesion and the blurred lesion serves as an indicator of malignancy [25]. This can be expressed as Equation 5.

$$\textit{Degree of spiculation} = \frac{\textit{area of unprocessed lesion} - \textit{area of blurred lesion}}{\textit{area of unprocessed lesion}} \tag{5}$$

2.3 Dynamic contrast-enhanced MRI

Dynamic contrast-enhanced MRI (DCE-MRI) of the breast has been shown to be the most sensitive technique in the detection of invasive breast cancer and is not limited by the density of the breast tissue [6,26]. The inherent MR contrast of the breast, as a result of the principles of proton nuclear magnetic resonance, is not sufficient on its own to distinguish normal tissue from cancer. Therefore, the use of an intravenous contrast agent (gadolinium-based) is necessary for better detection of breast tumors. The DCE-MRI will reflect the neovascularity of the lesion.

Studies have shown that angiogenesis is necessary for the growth of malignant tumors. Histopathology can show increased vascularity with the help of microscopy, and recent developments in immunohistopathology have shown that angiogenesis is quite a common factor seen in imaging modalities, such as DCE-MRI, that can image the presence of neovascularization well [22].

Malignant tumors are characterized by the formation of abnormal and leaky microvessels in the lesion. When an intravenous contrast agent is added it will pool in the interstitial spaces within the lesion. This is also true for some benign lesions, thereby creating an overlap in the appearance of benign and malignant lesions. Careful evaluation of lesion kinetics following contrast injection is needed to improve the specificity of MRI of the breast; cancerous lesions tend to enhance rapidly (so called wash-in) and then decrease (so called wash-out), whereas benign lesions tend to slowly and progressively enhance [27] (Figure 7).

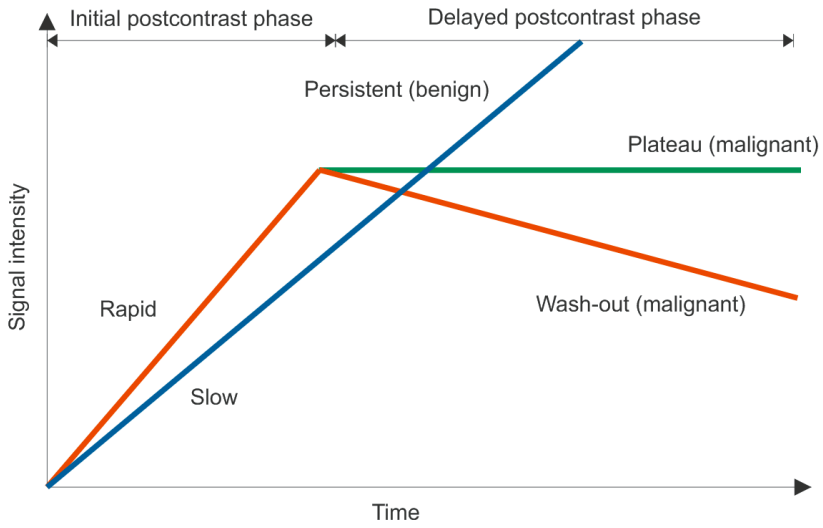

Figure 7: Illustration of time-signal intensity curve types and likely histology. (Ikeda D.M [28])

2.3.1 DCE-MRI evaluation using DynaCAD

The enhancement characteristics have been evaluated using a DynaCAD workstation (Invivo, Orlando, USA). After the MRI acquisition, the images are sent to DynaCAD for dynamic contrast uptake evaluation (Figure 8). The upper image in Figure 8 contains the information of the whole DCE-MRI series and is explained in more detail below. The contrast uptake curve (yellow), in the lower image of Figure 8, is a plot of the signal intensity (SI) as a function of time points (TP). SI is calculated in each voxel as $SI = [(SI_{post} - SI_{pre}) \times 100]/SI_{pre}$, where SI_{pre} is the intensity of signal previous to the contrast injection and SI_{post} is the measured intensity of signal after administration of contrast.

Small arrowheads can be placed on the x-axis to calculate different measures of the contrast curve. One arrowhead is set on TP1, furthermost to the left, representing the pre-contrast sequence. Another arrowhead is placed on TP3, representing the second post-contrast sequence. Finally a third arrowhead, TPx, is set at the last time point and marks the end of the contrast sequence.

The first two arrowheads measure the period of rapid enhancement and are chosen to catch the peak of the contrast curve of most malignant tumors. The baseline threshold for rapid enhancement, also called wash-in, is shown on the y-axis on the left side of the graph window. The bottom tic mark is set to 50% and indicates that between TP1 and TP3, there needs to be at least 50% change in signal (wash-in) in order for a pixel in the upper image of Figure 8 to change color. The upper tic, set to 150%, indicates that if the wash-in reaches that level, the color displayed will be brighter. For instance, if the second arrowhead is set to TP2 instead of to TP3, it will be very likely that only aggressively enhancing structures like heart, lymph nodes and maybe a few lesions will be the only things colored. By leaving the second arrowhead at TP3, it increases the likelihood of colorization to display more structures.

It is between TP3 and TPx that the delayed contrast phase, also in general called wash-out

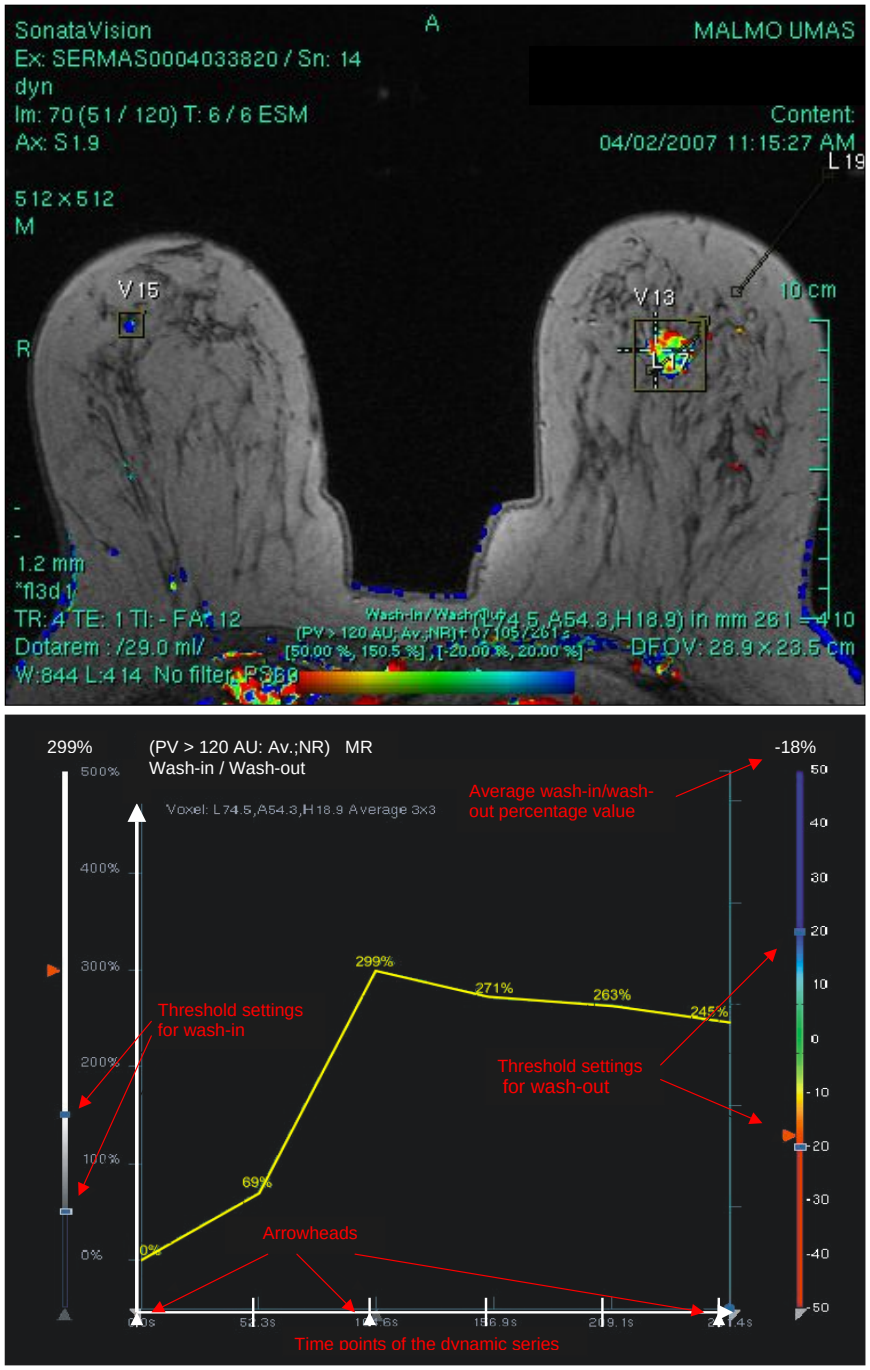

Figure 8: Upper image show a lesion with contrast enhancement. Lower image, that arise from the cross-hair indicated in the upper image, show a rapid enhancement followed by wash-out. The time span between two time points is roughly 50 seconds.

(not to be confused with the specific wash-out curve type mentioned in Figure 7), is measured and determines which color gets displayed in the upper image of Figure 8. The threshold settings for wash-out are set on the y-axis on the right side of the graph window. There are tic marks set at +20% and -20%. This is the averaged percentage of change between TP3 and TPx. If there is > 20% increase, the curve will display persistent enhancement, and the pixel will turn blue. If the average is within ±20% change over time, the pixel can be any one of the gradient colors shown on the y-axis on the right side of the graph window (green, yellow, orange). The curve will then portray a plateau. The final curve type is the wash-out curve that shows a greater than -20% difference in change and the pixel will be red in color. The average wash-in/wash-out percentage value is displayed at the very top of the color scale and it is the average between TP3 and TPx (Equation 6, 3.2).

Another tool in DynaCAD is the volume histogram function (Figure 9). The volume histogram displays the proportional distribution of all colorized voxels of the defined volume surrounding the entire lesion (Figure 14, 3.2), helping the radiologist to determine whether the lesion is benign or malignant.

The information of all contrast uptake curve types is displayed as percentage values. For instance, those voxels that have a rapid wash-in value > 150% and at the same time a wash-out < -20% are gathered in the upper left area. These voxels represent the wash-out type curve and are highly suggestive of malignancy. Those voxels that fit in the lower left area also refer to the wash-out type curve, but have a slower wash-in. A high percentage value in the lower right area, characterized by slow wash-in and a wash-out value > 20%, likely represents benign lesions [29].

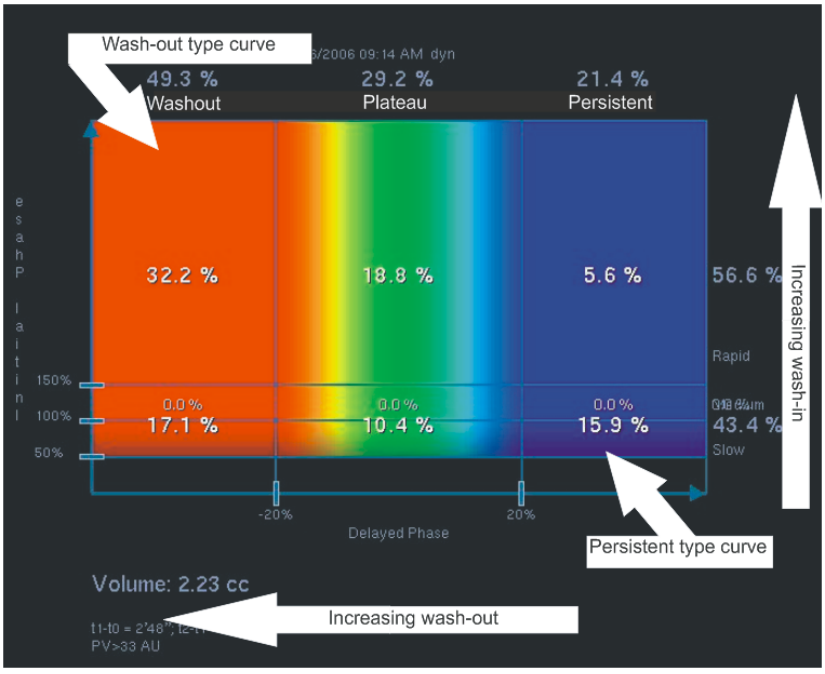

Figure 9: Example of a volume histogram of a malignant lesion. The percentage values of wash-out, plateau and persistent contrast uptake curve types are displayed. The large arrows also indicate increased wash-in and wash-out, respectively.

3 Materials and methods

As already indicated in Figure 5, a highly spiculated margin and irregular shape is related to a higher probability of malignancy. The purpose of this work is to quantify physical metrics of breast tumors in both BT and MRI images, compare the values and then investigate whether these metrics are suitable in predicting malignancy or not.

The material for this work consists of MRI and BT images from 10 patients who have undergone examinations using both modalities. The criterion for inclusion is the presence of a breast lesion (malignant or benign). In addition there are 16 specimen samples of malignant breast lesions, only examined with BT, that are used with the purpose to determine metrics of interest.

The malignancy grading was retrieved from the pathology report.

3.1 Development of BT metrics

A prototype BT unit (Siemens, Erlangen Germany) was used to acquire tomosynthesis images of specimens and patients. The beam quality used was determined by the automatic exposure control (AEC) of a full field digital mammography (FFDM) system (Mammomat Novation, Siemens, Erlangen Germany) [30]. The anode/filter combination was W/Rh and the tube loading used for the entire tomosynthesis scan was twice that of a single-view mammogram (for the specimens it was four times that of a single-view). The tube loading is divided equally among the 25 projection images acquired over a range of roughly 50°. Post-processing was performed on the measured projections and slices were reconstructed using filtered backprojection.

The tomosynthesis images were evaluated with the open-source software package ImageJ [31] using various plug-ins.

The outline of the mass lesion was obtained using a cell outliner plug-in originally developed to outline cell spreading [32]. Given a seed point, the technique helps to analyze contiguous areas as a function of gray level increment, where the gray level increments yield contours of potential lesion margins. An example of a mass lesion outline is provided in Figure 10 and the outline results have been shown to and verified by an experienced breast radiologist.

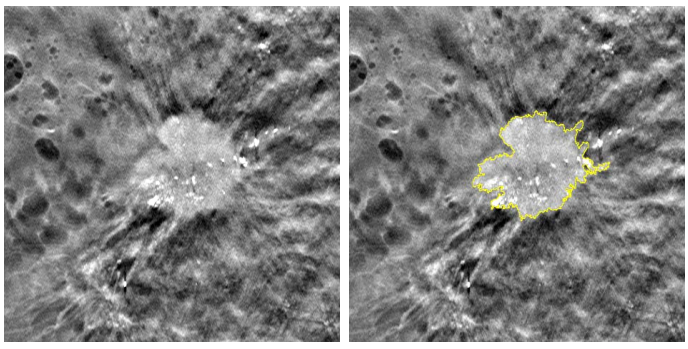

Figure 10: Example of mass lesion outline. The outline is shown in the right image. The original image is displayed to the left.

The outline was stored as a region of interest (ROI). Given a ROI, several measures can be calculated with ImageJ. In order to calculate the desired lesion characteristics, discussed in 2.2.1, the *fit ellipse* function is used. *Fit ellipse* replaces an area selection with the best fitting ellipse by using the headings major, minor and angle, where major and minor are the primary and secondary axes of the best fitting ellipse and angle is the angle between the primary axis and a line parallel to the x-axis of the image. The ellipse will have the same area, orientation and centroid as the original selection.

The required measures, area and perimeter, are obtained for the selected ROI through the *measure* option in ImageJ. The measure *area of potential mass within effective ellipse* is obtained by clearing everything outside the ROI, applying *fit ellipse* and again clearing everything outside the ellipse. Geometric features related to lesion shape, irregularity and ellipticity can then be calculated, according to Equations 1 and 2.

As mentioned in 2.2.1 the margin information of a lesion is obtained by morphological filtering using sequences of dilation (circular kernel of radius 2 pixels), erosion (circular kernel of radius 8 pixels, and dilation (circular kernel of radius 6 pixels) [25]. This is done using a morphology plug-in [33]. The initial dilation process is performed in order to maintain the connectivity of small spicules. The blurring process is illustrated in Figure 11. Note how the spicules in the margin are smoothed out. The degree of spiculation for the specimens and the patient images is calculated with Equation 5.

Figure 11: The original lesion (binary representation) is displayed before (left) and after (right) the process of blurring using a morphologic filtering sequence of dilation, erosion and dilation.

In addition the size was measured for all malignant mass lesions. The size (largest diameter) was obtained from the respective outline ROI through the *measure* option in ImageJ.

The sensitivity and specificity was also calculated for the BT and DCE-MRI metrics. Sensitivity is defined as true positive cases divided by true positive and false negative cases. Specificity is defined as true negative cases divided by true negative and false positive cases. The threshold value determines whether it is a positive or negative case. If it is true or false is given by the PAD.

A Student's t-test was performed to test whether the difference between mean values of the various metrics between malignant and benign cases were statistically significant. A p value less than 0.05 indicated that the differences were statistically significant at the 5% level.

3.2 Development of DCE-MRI metrics

The breast MR examination was performed on a 1.5 T MRI scanner (Magnetom SonataVision, Siemens, Erlangen, Germany) with the patient in head first prone position, using a dedicated bilateral breast coil. A standardized "mammo-routine" protocol was used. An initial localizer view provides axial, coronal and sagittal images of the left and right breast. These scout images are used to accurately localize the spatial distribution of the parenchymal volume in both breasts. This is followed by a morphologic T2-weighted turbo spin-echo sequence, with repetition time 6250 ms and echo time 101 ms. When the sequence is finished the administration of the contrast agent begins. An intravenous bolus of 0.4 mmol of gadopentetate dimeglumine (Dotarem, Guerbet, France) per kilogram of body weight is injected, immediately followed by a 20 ml saline solution flush. A dynamic T1-weighted fast 3D-spoiled gradient-echo sequence starts simultaneously with the administration of the contrast agent. The contrast lowers the T1-relaxation time and hence, tissue areas that absorb the contrast will shine bright. The imaging parameters for the T1-weighted sequence are: TR/TE=4.3 ms/1.46 ms: flip angle 12°: and FOV (Field of View) 320 mm with a 512x512 matrix. The whole sequence scan time is 4:34 min, where each dynamic scan takes roughly 50 s, and the slice thickness is 1.2 mm. The dynamic series consists of seven individual dynamic image volumes; one obtained before and six after the bolus injection. Finally a sagittal flash 3D sequence is performed as a complement. Postprocessing includes image subtraction of the dynamic series and a maximum intensity projection (MIP) reconstruction of the subtracted dynamic images.

After the routine protocol, all breast images were sent to the DynaCAD workstation where the evaluation of the dynamic contrast uptake curves was performed. The images underwent a smoothing process using a 3 x 3 averaging kernel, in order to reduce noise. An example of how the contrast uptake varies within the lesion is shown in Figure 12. Usually an inhomogeneous uptake is seen and in order to quantify the enhancement rate, a consistent measure method for all mass lesions is needed. Hence, the crosshair placement was done using the *enhancement rate* mode in the program. Selecting this mode will create a color gradient map of the most enhancing parts within the breast (Figure 13). By setting a threshold level, the maximum enhancing area within the lesion at TP3 will be displayed as red.

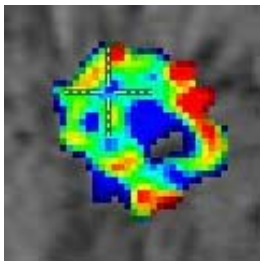

Figure 12: Example of contrast uptake within a lesion. Typically a high rim enhancement is seen for malignant tumors.

With the crosshair placed at the pixel with maximal initial enhancement, the display mode is switched to wash-in/wash-out. The final curve type of the lesion is then obtained. The

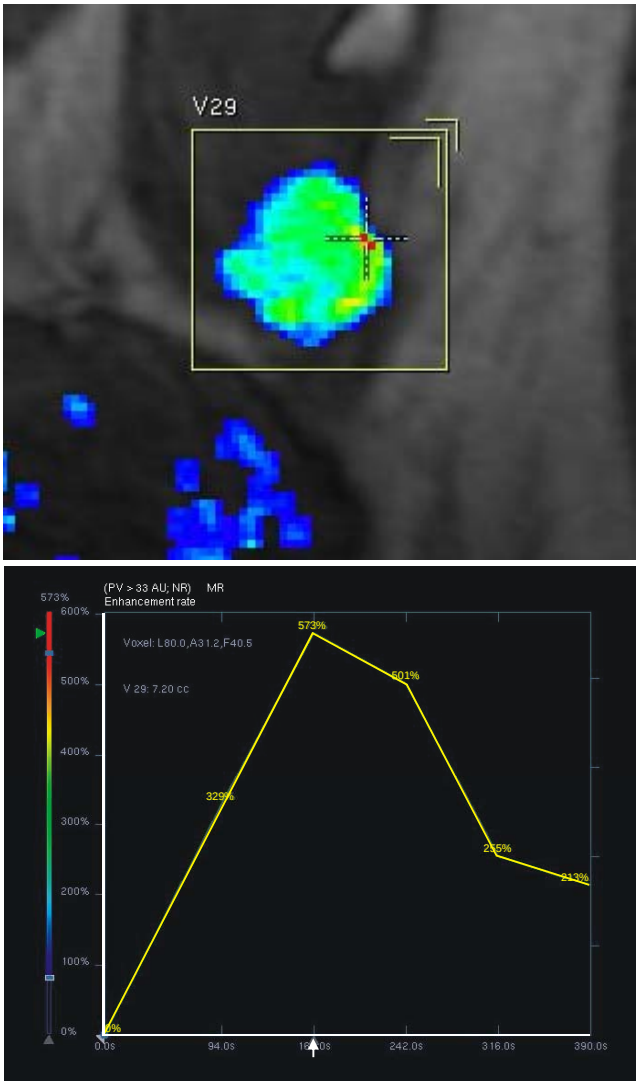

Figure 13: The upper image shows the enhancement rate within the lesion at TP3. By setting a threshold value the maximum enhancement will be displayed as a red pixel. The lower image shows the resulting contrast uptake curve.

average wash-in/wash-out percentage value, as mentioned in 2.3.1 and illustrated in Figure 8, is the quantitative value being used for analysis. It is calculated according to the wash-in/wash-out Equation 6.

$$wash\text{-}in/wash\text{-}out = \left(\frac{TPx}{TP3} - 1\right) * 100 \tag{6}$$

The volume histogram is acquired by manually enclosing the mass lesion within a rectangular prism (Figure 14). This is done by viewing the sagittal, coronal and axial images of the lesion and adjusting the volume of interest to cover the whole lesion. The volume histogram will relate the histology of a lesion with the percentage of a specific curve type. Since malignant lesions can both have plateau and wash-out appearance, the percentage of the voxels that represent persistent curve type (benign lesions), was used.

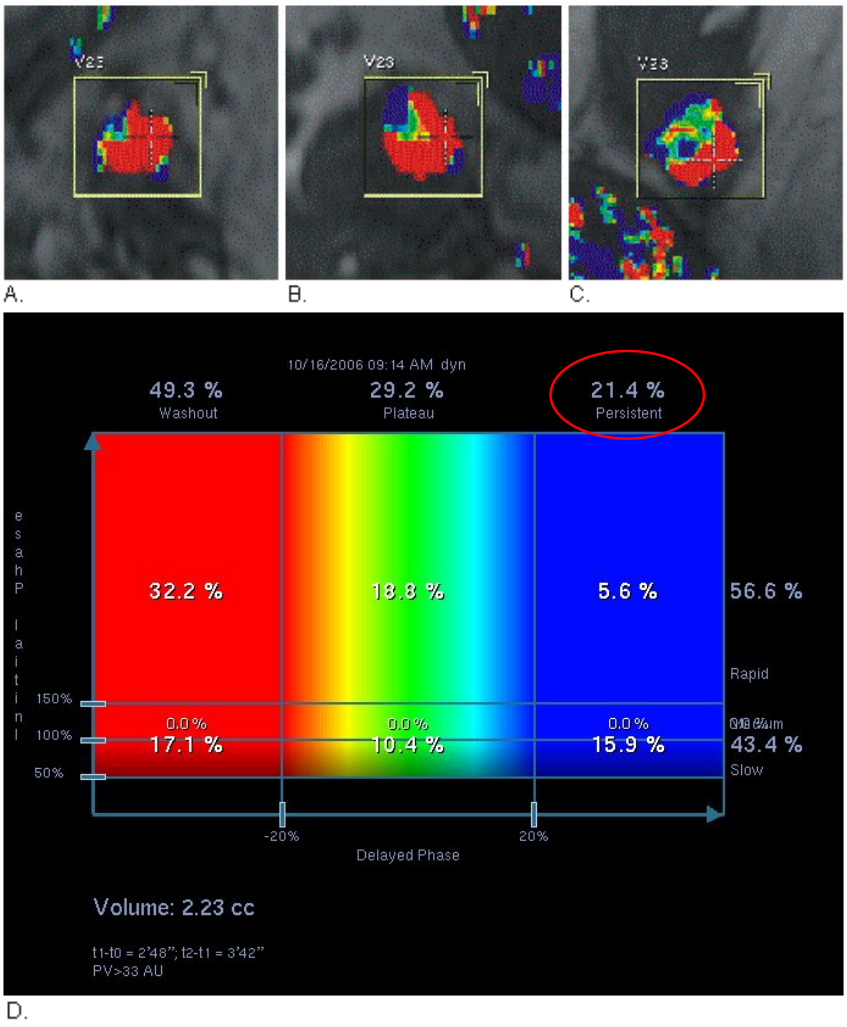

Figure 14: (A) Coronal view. (B) Sagittal view. (C) Axial view. (D) Volume histogram of a malignant lesion with the persistent curve type percentage indicated.

4 Results

4.1 Development of BT metrics using breast specimens

The data of geometric features related to the margin and shape of the lesion obtained with BT for the specimen samples, are summarized in Table 2. The PAD and size of the respective lesion are also shown in the table.

Table 2: Lesion PAD related to characteristics of the lesion obtained with BT for the specimen samples.

PAD	Size	Irregularity	Ellipticity	Degree of spiculation
9 mm DCIS gr1	11 mm	0.62	0.80	0.033
10 mm IDC gr1	18 mm	0.50	0.90	0.052
12 mm IDC gr1	13 mm	0.48	0.72	0.056
15 mm IDC gr1	19 mm	0.36	0.94	0.009
35 mm IDC gr1	16 mm	0.57	0.84	0.016
11 mm IDC gr2	11 mm	0.19	0.93	0.010
11 mm IDC gr2	12 mm	0.52	0.84	0.030
12 mm ILC gr2	11 mm	0.48	0.90	0.026
15 mm ILC gr2	17 mm	0.65	0.85	0.067
16 mm IDC gr2	17 mm	0.56	0.89	0.039
17 mm IDC gr2	17 mm	0.65	0.85	0.017
17 mm IDC gr2	22 mm	0.73	0.79	0.020
20 mm IDC gr2	22 mm	0.42	0.90	0.012
22 mm IDC gr2	25 mm	0.75	0.78	0.022
16 mm IDC gr3	16 mm	0.69	0.78	0.090
20 mm IDC gr3	22 mm	0.73	0.80	0.036

IDC: invasive ductal carcinoma, *ILC*: invasive lobular carcinoma, *DCIS*: ductal carcinoma in situ

Figures 15, 16 and 17 shows how the geometric features of the margin and shape of a lesion are related to lesion grade. Grade 3 lesions have higher irregularity and degree of spiculation, but lower ellipticity averages compared to grade 1 and 2 lesions. In Figure 15 grade 3 lesions seem to be separable from grade 1 lesions. However, in general there is no relationship between the geometric features of the margin and shape of a lesion and lesion grade.

Another important matter is that the lesions have only been evaluated two-dimensionally in the x-y plane and not in the z plane. The impact of how the BT metrics vary with the z plane has also been investigated. Table 3 shows how the BT metrics vary for a malignant lesion in five different z planes. One slice represents roughly 1 mm and as can be seen from the table, the differences between the parameter values are small. The reason why the degree of spiculation is so high in slice 37 is because a spicule was completely removed in the erosion process.

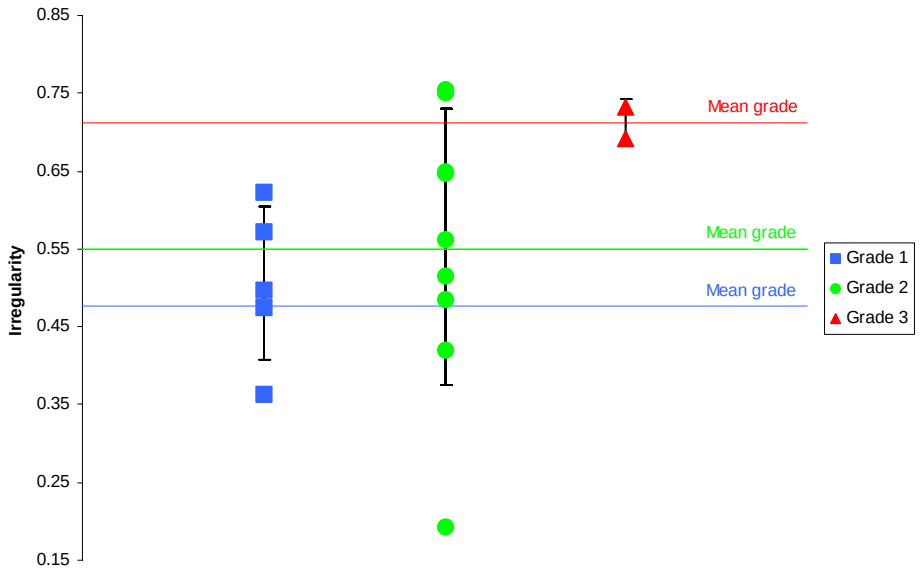

Figure 15: Plot of irregularity vs. lesion grade. The error bars denote one standard deviation.

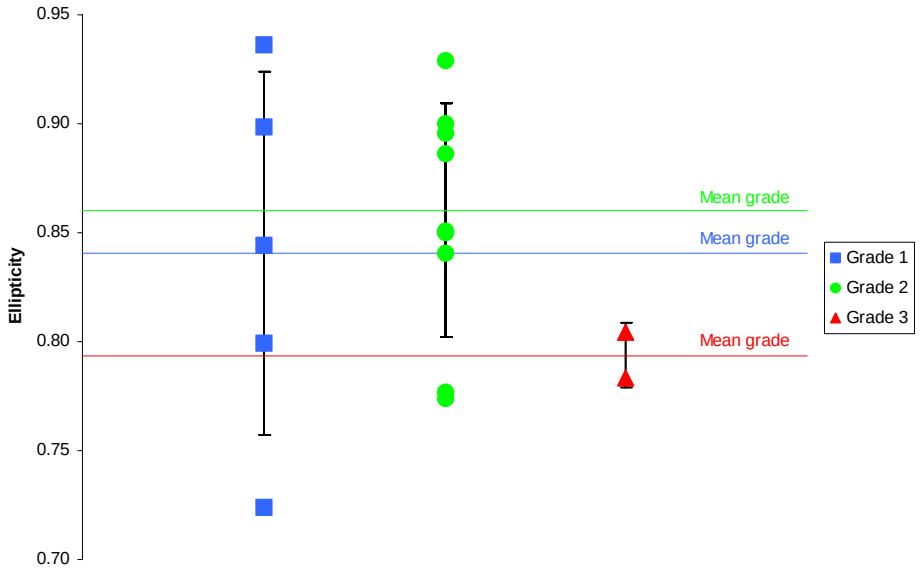

Figure 16: Plot of ellipticity vs. lesion grade. The error bars denote one standard deviation.

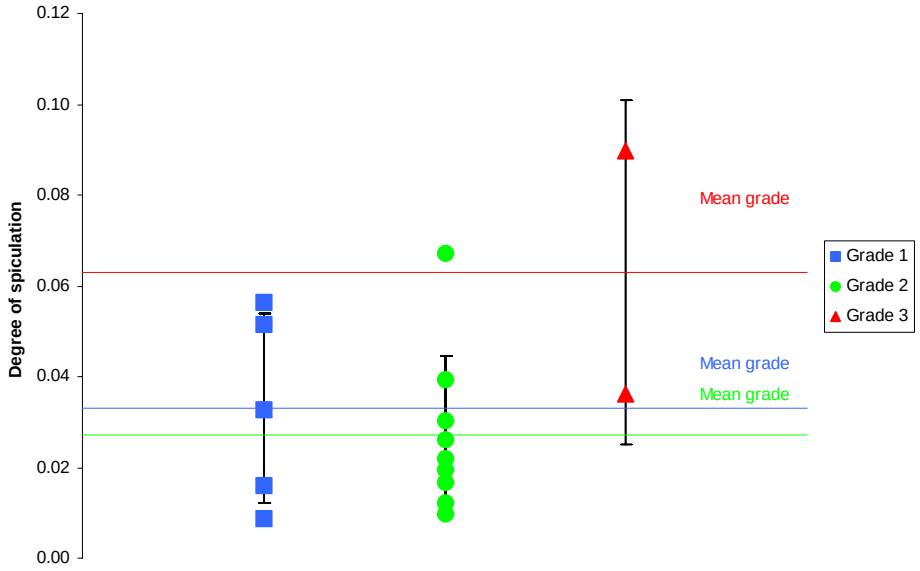

Figure 17: Plot of degree of spiculation vs. lesion grade. The error bars denote one standard deviation.

Table 3: Example of how the z-dimension influences the characteristics of a lesion obtained with BT (MV = mean value, SD = one standard deviation).

Z-slice	Size	Irregularity	Ellipticity	Degree of spiculation
37	27 mm	0.83	0.84	0.023
39	30 mm	0.74	0.83	0.003
41	29 mm	0.73	0.83	0.003
43	28 mm	0.75	0.79	0.006
45	28 mm	0.69	0.81	0.001
	MV 28 mm	MV 0.75	MV 0.82	MV 0.007
	SD 1 mm	SD 0.05	SD 0.02	SD 0.009

4.2 Development of DCR-MRI metrics for patient population

Ten lesions were seen in the MRI images of the patient population. The wash-in/wash-out and the persistent curve type percentage values of the lesions are summarized in Table 4.

Table 4: Lesion PAD with respective values of wash-in/wash-out and persistent curve type percentage.

PAD	wash-in/wash-out	persistent curve type percentage
Benign lesion	-25%	23.7%
Benign lesion	-1%	72.2%
Benign lesion	34%	83.1%
Benign lesion	36%	92.6%
8 mm IDC gr2[a]	-15%	38.3%
17 mm IDC gr2[a]	-63%	21.4%
20 mm ILC gr2	-21%	38.5%
10 mm IDC gr3	-2%	23.3%
24 mm IDC gr3	-30%	27.6%
28 mm IDC gr3	-3%	NA[b]

[a] Not visible in the BT examination.
[b] Half of the dynamic series got deleted, hence no persistent curve type percentage could be calculated for this tumor.

Figure 18 shows the relationship between lesion type and DCE-MRI metrics. There is an overlap between malignant and benign lesions for both methods. However, the persistent curve type percentage seems to have a better grouping of the malignant and benign lesions, respectively, with one exception. In general malignant lesions tend to have a persistent curve type percentage value between 20-40% and a negative wash-in/wash-out value.

The sensitivity and specificity have also been calculated for the DCE-MRI metrics (Table 5). The threshold values are set to 0% and 50%, respectively. A wash-in/wash-out value equal to or below 0% refers to a plateau or wash-out curve type and a value of 50% is set for the persistent curve type percentage, simply referring to the majority percentage share.

Table 5: Sensitivity and Specificity

Method	Threshold value	Sensitivity	Specificity
Wash-in/wash-out	0%	100%	50%
Persistent curve type percentage	50%	100%	75%

Both methods have a sensitivity of 100% but the specificity is higher for the persistent curve type percentage method, given the threshold values.

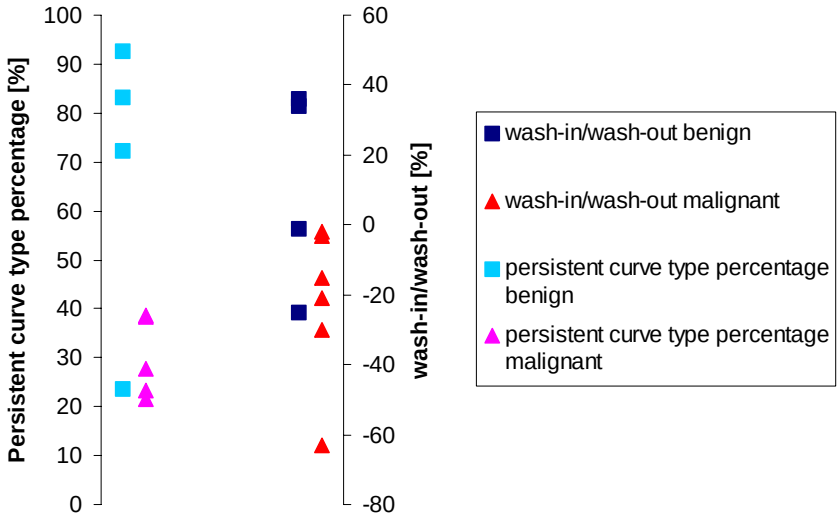

Figure 18: Relationship between lesion type and DCE-MRI metrics. (There is an overlap between malignant and benign lesions for both methods. However, the persistent curve type percentage seems to have a better grouping of the malignant and benign lesions, respectively, with one exception)

- p = 0.085 was obtained for persistent curve type percentage between malignant and benign lesions.
- p = 0.194 was obtained for wash-in/wash-out between malignant and benign lesions.

Consequently, no significant difference was found for the DCE-MRI metrics.

4.3 Application of developed BT metrics to patient population

Only 8 out of 10 lesions in the patient population were seen in both the MRI and BT images. An 8 mm IDC gr2 and a 17 mm IDC gr2 were not seen in the BT images.

The data of the geometric features related to the margin and shape of the lesion obtained with BT for the patient population are summarized in Table 6. The PAD and size of the respective lesion are also shown in the table.

Table 6: Lesion PAD related to characteristics of the lesion obtained with BT for the patient group.

PAD	Size	Irregularity	Ellipticity	Degree of spiculation
Benign lesion	7mm	0.19	0.94	0.006
Benign lesion	7mm	0.26	0.92	0.065
Benign lesion	10mm	0.42	0.93	0.012
Benign lesion	12mm	0.53	0.88	0.010
20 mm ILC gr2	14mm	0.73	0.78	0.051
10 mm IDC gr3	12mm	0.66	0.76	0.056
24 mm IDC gr3	28mm	0.73	0.83	0.003
28 mm IDC gr3	38mm	0.70	0.83	0.013

Since no relationship was found between the geometric features of the margin and shape of a lesion and lesion grade, no sort of predictiveness is further investigated. However, the sensitivity and specificity are summarized in Table 7. The threshold values were set arbitrary to yield the highest sensitivity.

Table 7: Sensitivity and Specificity

Method	Threshold value	Sensitivity	Specificity
Irregularity	0.60	100%	100%
Ellipticity	0.85	100%	100%
Degree of spiculation	0.012	75%	75%

Both irregularity and ellipticity have 100% sensitivity and specificity, given the threshold values.

- p = 0.002 was obtained for irregularity between malignant and benign lesions.
- p = 0.017 was obtained for ellipticity between malignant and benign lesions.
- p = 0.709 was obtained for degree of spiculation between malignant and benign lesions.

A significant difference was found for the metrics irregularity and ellipticity.

4.4 Inter-metric analysis (BT-MRI) of patient population

Inter-metric analysis was performed in order to investigate if lesion characteristics such as irregularity could depend on increased angiogenesis. The relationship between MRI wash-in/wash-out values and BT values of geometric features related to the margin and shape of the lesion is presented in Figures 19, 20 and 21. No relationship was found in the inter-metric analysis. However, if more data was available there could be a tendency of a linear relationship between MRI wash-in/wash-out and irregularity in Figure 19.

How irregularity and ellipticity are able to differentiate between malignant and benign lesions, is clearly seen in Figures 19, 20.

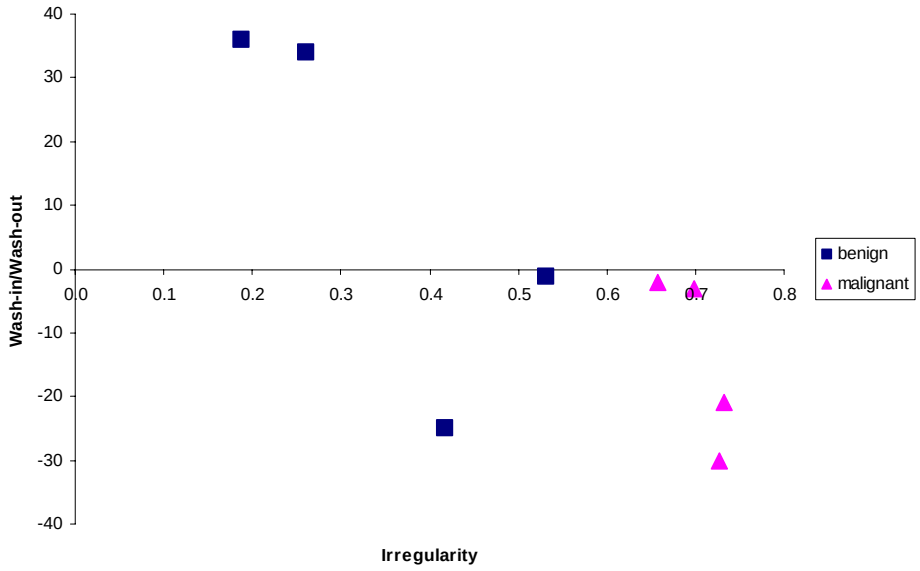

Figure 19: Relationship between MRI wash-in/wash-out values and BT irregularity values for the patient population.

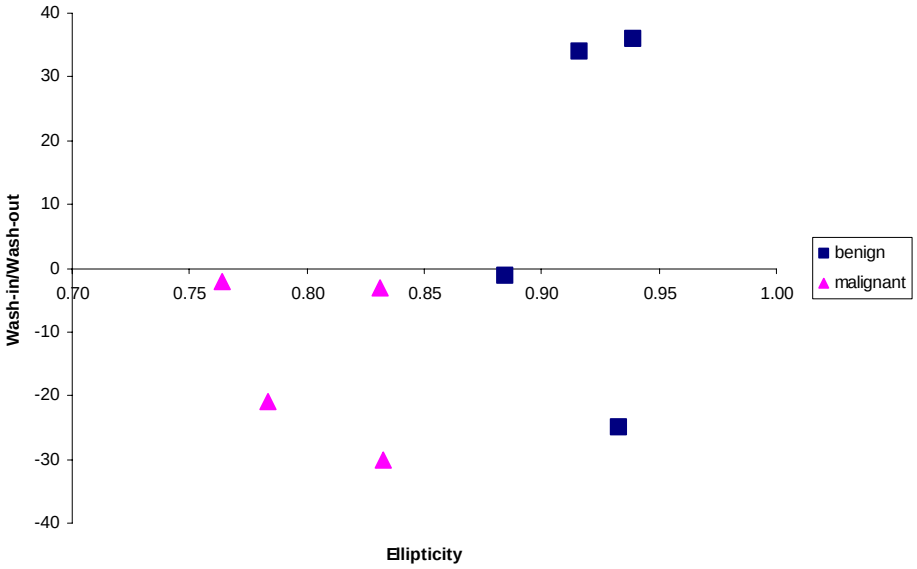

Figure 20: Relationship between MRI wash-in/wash-out values and BT ellipticity values for the patient population.

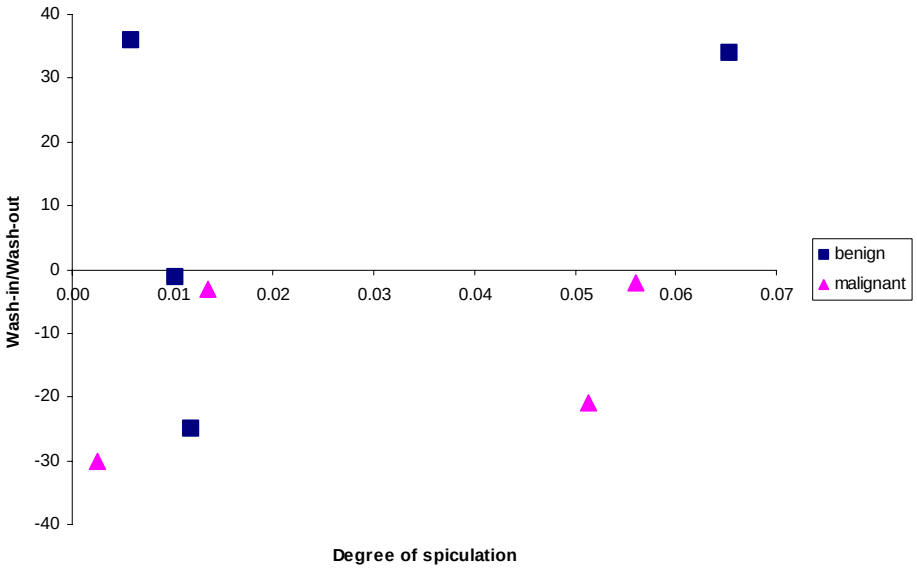

Figure 21: Relationship between MRI wash-in/wash-out values and BT degree of spiculation values for the patient population.

5 Discussion

This work has been based around obtaining the characteristic geometric features of lesions using new approaches. Irregularity, ellipticity and degree of spiculation are all described in the literature [18,25] and are here presented in a novel way using plug-ins for ImageJ. Two ways of calculating DCE-MRI parameters are also provided.

With regards to the specimen section of this work, the objective was to establish a baseline performance metric for tumor characteristics in BT images. The specimen BT images were taken with four times higher tube loading than the patient population BT images, and this increases the contrast-to-noise ratio, but could also affect the metric results. However, the idea of the introduction of specimens was to create higher image quality to establish good metrics. Since the specimens represent a larger sample size and more specific characteristics, they are assumed to work as a baseline in a noisy smaller sample of patient images. This model could potentially be used, however with the current data no conclusions can be drawn regarding the relationship between lesion grade and geometric features related to margin and shape of the lesion. The reason for the investigation was the hypothesis that more "aggressive" tumors have a more "aggressive" growth pattern. This has been disputed by Ingvar Andersson, who has the impression that the opposite is true. It could be the case that the metrics used in this lesion grade study do not capture the needed characteristics, or that not enough data was available, to confirm a relationship in one way or the other.

The BT metrics have been developed with the purpose to separate malignant from benign lesions. The grade of a lesion is intrinsically linked to malignancy and although no relationship can be established between the BT metrics and tumor grade this does not affect the differentiation between malignant and benign lesions.

It is somewhat uncertain to do a comparison of specimen and patient population values. This is demonstrated by the fact that the obtained patient population threshold values are not applicable for the specimens. If this is a result due to lack of data or different acquisition settings is hard to tell, but to resolve this problem one would also have to include a study of benign specimens. Unfortunately that data was not available.

No mean filter was used on the images and this is the reason why the parameter *degree of spiculation* seems to have very fluctuating values, particulary for the patient population. The margin was very noisy and small pixel fluctuations would alter the margin outline affecting the acquired degree of spiculation values.

The development of the DCE-MRI metrics (*wash-in/wash-out, persistent curve type percentage*) was disturbed by the fact that the scanning protocol was changed twice during the metrics collection of the patient population. This resulted in a different amount of time points but also the time span between the time points was affected. This has an impact on the generation of dynamic contrast curves, thus affecting the parameter values. The optimum would be to have as high temporal resolution as possible, but apart from that there has to be an optimal setting to differentiate malignant from benign lesions. The diagnostic value of the early phase enhancement and late post contrast phase criterion is still under investigation in order to find an optimal setting to differentiate malignant from benign lesions. In addition, also the threshold settings as mentioned in 2.3.1, which determine how the lesion is depicted in the MRI images, need to be investigated further.

The dynamic contrast uptake curve arises from one voxel as mentioned earlier in the text. In order to reduce errors that could influence the results a smoothing convolution filter was

applied to reduce noise and movement artifacts were considered to have a low impact on the error. The introduction of the measure persistent curve type percentage would overcome the problem that the whole measurement is dependent on only one voxel, as it takes all voxels of the lesion into consideration. The persistent curve type percentage result also implies that this is a more robust measure, than the wash-in/wash-out measure, where some of the data points are in the vicinity of the threshold value.

In the inter-metric analysis of the patient population, all 10 lesions were seen in the MRI images but only 8 were seen in the BT images. This suggests that the general sensitivity is higher for MRI. The background for the inter-metric analysis was to see if lesion characteristics such as irregularity could depend on increased angiogenesis. Not enough data was available to draw any conclusions and this is also the reason why only wash-in/wash-out was compared to the BT metrics, as even less data existed for the persistent curve type percentage. The BT and MRI examinations were usually taken within three weeks, however a few have longer time apart. During that time the characteristics of the lesion could change.

The most critical measure in this work is the tumor outline, since all other geometric measures are obtained from it. As mentioned before, the tumor outlines have been shown to an experienced radiologist and considered acceptable. The difficult task is to know exactly what tissue is actually malignant. Thin malignant spicules could be missed in the tumor outline, but also thick spicules could be cut off at a certain length. Nevertheless, with a few exceptions, the tumor outline sizes tend to agree with the PAD sizes.

Another important matter is that the lesions have only been evaluated two-dimensionally in the x-y plane and not in the z plane (Table 3). This could have an impact on threshold values selection when calculating sensitivity and specificity for the BT measures. Also, which applies to the whole study, not enough data was available to draw real conclusions.

The most important finding in this work is that it is possible to differentiate between malignant and benign breast tumors using the measures irregularity and ellipticity. However, at this point in time, it is too complicated to apply this method in the everyday clinical work. CAD (Computer-Aided Diagnosis) programs do exist and are commercially available. In the development of such programs, the type of measures presented here could be taken into account amongst other parameters.

6 Conclusion

In this pilot study, MRI metrics and geometric features related to the margin and shape of the lesion obtained with BT, were investigated. Two different DCE-MRI metrics have been established and compared. The results indicate that the BT parameters *irregularity* and *ellipticity* may be useful for differentiation between malignant and benign tumors.

7 Acknowledgements

I would like to thank Mark Ruschin who initiated this project giving me the great opportunity to work with tomosynthesis and MRI. His comments and criticism have been of great guidance during the progress of the project. My supervisor Anders Tingberg for all the support and suggestions. Jonas Svensson for helping me with the MRI part. Ingvar Andersson and Marianne Löfgren who took great time to help me and provided me with their expertise in mammography. Finally I would like to thank Tony Svahn and Pontus Timberg, who always had time for me and provided me with support, material and most of all great enthusiasm.

References

[1] Socialstyrelsen (2005) http://www.socialstyrelsen.se/Statistik/

[2] Andersson I, *et al.* (1988) "Mammographic screening and mortality from breast cancer: the Malmo mammographic screening trial." *Bmj* **297** 943-948

[3] Nyström L, *et al.* (1993) "Breast cancer, screening with mammography: overview of Sweish randomised trials." *Lancet* **341** 973-978

[4] Bissonnette M, *et al.* (2005) "Digital breast tomosynthesis using an amorphous selenium flat panel detector." *Proc SPIE* **5745** 529-540

[5] Timberg P, *et al.* (2008) "Impact of dose on observer performance in breast tomosynthesis using breast specimens." Accepted for publication in *SPIE*

[6] Kuhl C K, *et al.* (2007) "Current status of breast MR imaging. Part 2. Clinical applications." *Radiology* **244** 672-691

[7] Heywang S H, *et al.* (1989) "MR imaging of the breast with Gd-DTPA: use and limitations." *Radiology* **171** 95-103

[8] Kaiser W A, *et al.* (1989) "MR imaging of the breast: fast imaging sequences with and without Gd-DTPA. Preliminary observations." *Radiology* **170** 681-686

[9] Lord S J, *et al.* (2007) "A systematic review of the effectiveness of magnetic resonance imaging (MRI) as an addition to mammography and ultrasound in screening young women at high risk of breast cancer." *Eur J Cancer* **43** 1905-1917

[10] Kuhl C K, *et al.* (2005) "Mammography, breast ultrasound, and magnetic resonance imaging for surveillance of women at high familial risk for breast cancer." *J Clin Oncol* **23** 8469-8476

[11] Dobbins J T 3rd, *et al.* (2003) "Digital x-ray tomosynthesis: current state of the art and clinical potential." *Phys Med Biol* **48** R65-R106

[12] Mertelmeier T, *et al.* (2006) "Optimizing filtered backprojection reconstruction for a breast tomosynthesis prototype device." *Proc SPIE* **6142** 131-142

[13] Mammomat Novation^{DR} Manual (2007) Siemens AG, Germany

[14] Svahn T, *et al.* (2007) "In-plane artifacts in breast tomosynthesis quantified with a novel contrast-detail phantom." *Proc SPIE* **6510** 65104R

[15] Niklason L T, *et al.* (1997) "Digital tomosynthesis in breast imaging." *Radiology* **205** 399-406

[16] Ruschin M, *et al.* (2007) "Improved in-plane visibility of tumors using breast tomosynthesis." *Proc SPIE* **6510**, Physics of Medical Imaging 65101J

[17] Andersson I (2005) "Invasive breast cancer." *Radiologic-Pathologic Correlations from Head to Toe*, Springer 757-766

[18] Giger M L, *et al.* (2000) "Computer-aided diagnosis in mammography." *Handbook of Medical Imaging, Volume 2. Medical Image Processing and Analysis*, SPIE Press 915-1004

[19] Elston C W, *et al.* (1991) "Pathological prognostic factors in breast cancer. The value of histological grade in breast cancer: experience from a large study with long-term follow-up." *Histopathology* **19** 403-410.

[20] Dalton L W, *et al.* (2000) "Histologic grading of breast cancer: linkage of patient outcome with level of pathologist agreement." *Mod Pathol* **13** 730-735

[21] Azavedo E, *et al.* (1991) "Radiologic aspects of breast cancers detected through a breast cancer screening program." *Eur J Radiol* **13** 88-90

[22] Azavedo E (2005) "Breast Cancer: Correlations Between Imaging and Morphological Details." *Radiologic-Pathologic Correlations from Head to Toe*, Springer 785-789

[23] Kristoffersen Wiberg M, *et al.* (2003) "Comparison of lesion size estimated by dynamic MR imaging, mammography and histopathology in breast neoplasms." *Eur Radiol* **13** 1207-1212

[24] Boetes C, *et al.* (1995) "Breast tumors: comparative accuracy of MR imaging relative to mammography and US for demonstrating extent." *Radiology* **197** 743-747

[25] Giger M L, *et al.* (1994) "Computerized characterization of mammographic masses: analysis of spiculation." *Cancer Lett* **77** 201-211

[26] Fischer U, *et al.* (1999) "Breast carcinoma: effect of preoperative contrast-enhanced MR imaging on the therapeutic approach." *Radiology* **213** 881-888

[27] Kuhl C K, *et al.* (1999) "Dynamic breast MR imaging: are signal intensity time course data useful for differential diagnosis of enhancing lesions?" *Radiology* **211** 101-110

[28] Ikeda D.M, personal communication, 2007

[29] Federman S, DynaCAD, personal communication, 2007

[30] Bernhardt P, *et al.* (2006) "X-ray spectrum optimization of full-field digital mammography: Simulation and phantom study." *Med Phys* **33** 4337-4349

[31] Rasband W S, ImageJ, United States National Institute of Health, Bethesda, USA, http://rsb.info.nih.gov/ij/

[32] Castleman M, http://rsb.info.nih.gov/ij/plugins/cell-outliner.html

[33] Prodanov D, http://rsb.info.nih.gov/ij/plugins/gray-morphology.html